Porous alumina thin films on conductive substrates for templated 1-dimensional nanostructuring

N. Holubowitch, L. C. Nagle, and J. F. Rohan*

Tyndall National Institute

University College Cork

Cork, Ireland

***corresponding author (email: james.rohan@tyndall.ie, postal address: Tyndall National Institute, University College Cork, Lee Maltings, Cork, Ireland, Telephone: +353 21 490 4224)**

Abstract

The growth of thin porous anodic aluminum oxide (AAO) films on silicon by anodizing Al on Ti/Au/Si and Ti/Pt/Si substrates in oxalic acid was demonstrated. Removal of the Al_2O_3 barrier layer was effected by selective chemical etching in H_3PO_4 and a reversed bias method in the anodizing solution. Ion transport and the influence of the Ti adhesion layer at the oxide-metal interface during the critical stages of anodization and pore opening were investigated. The AAO films may be exploited as templates in the creation of silicon-integrated nanostructured wire arrays. Electrodeposition of Pt into the AAO template yielded a nanowire array with superior methanol oxidation activity that can be integrated in a micro direct methanol fuel cell.

Keywords

AAO template; Barrier layer; Ti adhesion layer; Si integration; Pt nanowire array; DMFC

Introduction

Anodic aluminum oxide (AAO) templates with sub-100 nm dimensions provide an inexpensive route for generating functional 1-dimensional nanostructures. It is desirable to deposit these structures on Si substrates for the integration of additional functionality with micro and nanoelectronic devices such as micro energy sources [1]. Microfabricated direct methanol fuel cells (μDMFC) are one such potential energy solution for systems integration [3-6].

Electrochemical conversion of Al to Al_2O_3 under anodic bias proceeds via electric field-induced oxide formation/dissolution at equilibrium, yielding a hexagonal well-ordered porous AAO template [7]. The concomitant electrically insulating barrier layer, however, is one of the main limitations to AAO technology and its selective removal has not yet been standardized, although progress has been made by several authors [8-16]. When anodizing Al as a thin film, on a multi-layered substrate with conductive interstitial layers, the final morphology of the barrier layer is heavily influenced by these underlying materials [17]. Therefore, investigation of this process is necessary on typical and versatile substrates such as Ti/Au/Si and Ti/Pt/Si. The electrode reactions occurring at the barrier layer-metal/Si interface are complex and need to be examined in detail. Zhao et al [18] offer a concise review of AAO template growth on multilayered Si-based substrates and the challenges involved in barrier layer removal. This process critically depends on the thickness of the Ti adhesion layer bonding Al to Au or Pt. Liu et al [19] recently elucidated the role of Ti in TiO_2 formation and barrier layer inversion upon anodizing Al on ITO substrates. Similarly, Asoh et al [16] transferred AAO's hexagonal honeycomb array pattern to substrates by anodization over Si. However, inclusion of conductive noble metal interlayers for further functionality has a non-trivial effect on the AAO-substrate interface and should therefore be investigated in detail. Furthermore, data are sparse on the influence of adhesion layers

required in these multilayered AAO substrates (especially on Si) and no consensus has been reached by the scientific community on barrier layer etching methods.

When this insulating layer is successfully and reproducibly etched, the barrier-free alumina template contains through-hole pores with tunable dimensions (by adjusting anodization bath composition and/or chemical etch duration [20]). The AAO thickness depends on the original deposited Al thickness (resultant AAO is slightly thicker due to volume expansion) and can be adjusted accordingly to achieve desired pore depths. Following these steps, electrodeposition of nanowires with customized dimensions into the pores is possible. We believe the findings herein contribute towards the understanding of AAO processing to assist with the realization of low-cost/high-yield nanostructure synthesis for commercial applications in nanotechnology.

Experimental

Si wafers were coated with 100 nm Au or Pt layers deposited by electron beam evaporation. The noble metal seed layer serves as an electrical contact, current collector and base for 1-D nanostructures. A 10 nm Ti adhesion layer followed by 2.5 μm Al were sputter deposited on top of the noble metal.

The as-deposited Al was anodized at 40 V in 0.3 M oxalic acid at 2 °C until all Al metal was converted to oxide, indicated by a color change revealing the underlying titanium. Five minutes overanodization was also applied to induce void formation underneath each pore. This resulted in an AAO template with highly ordered hexagonal pore morphology with inverted pore base (Figure 1). The single step anodization process is optimal for such thin films to retain thickness of deposited Al layer in AAO. The resulting template was 3.2 μm thick due to volume expansion. Pore widening was effected in 5wt.% H_3PO_4 at 40 °C to reach the desired pore

diameter, typically 10 min. The resulting pore density was on the order of 10^8 pores cm^{-2} and the pitch was 95 nm. Finally, electrochemical barrier layer etching exposed the underlying metal seed layer via reversed bias at -10 V in 0.3 M oxalic acid until bubbles emerge from template.

One possible application for these supported templates was explored by the electrochemical deposition of Pt into the pores for fuel cell catalysis. A commercial Pt-DNS bath (Metakem, containing 5 g Pt/l) at 60 °C and pH 2.5 was used for galvanostatic Pt deposition at 10 mA cm^{-2} to fill the pores after a 10 minute pre-soak period. The AAO template was then removed by chemical etching in 1 M NaOH at room temperature to reveal free standing Pt nanowire array. Cu and Ni wires were also deposited into the in-house templates via a similar method.

Micrographs were acquired by a Quantum FEG 650 field-emission scanning electron microscope. Electrochemical deposition and cyclic voltammetry experiments (CV) were performed with a CH Instruments 660C potentiostat supplied by IJ Cambria. CVs were recorded at room temperature with respect to the standard calomel reference electrode (SCE) using a platinized Ti mesh as counter electrode at a scan rate of 20 mV s^{-1}.

Results/Discussion

Upon anodization, ion transport from solution through alumina (native or barrier layer) converts Al and eventually the underlying Ti to oxide at the metal-oxide interface:

$$2Al^{3+} + 3H_2O \rightarrow Al_2O_3 + 6H^+$$

$$Ti + 2O^{2-}\ (4OH^-) \rightarrow TiO_2 + 4e^-\ (+ 2H_2O)$$

Figure 2 shows relative *I-t* curves during anodization of Al and reversed bias barrier layer etching. The anodization current is initially high (domain 1a) and quickly declines to a steady

state (porous Al_2O_3 formation/dissolution, domain 2a). The final stage of anodization (Fig. 2, domain 3a) is of particular interest and the evolution of a single pore through these critical steps is presented in Figure 3.

As the tip of the propagating porous alumina reaches the underlying metal, the strong electric field draws O^{2-} and OH^- anions through the oxide and begins to anodize the Ti adhesion layer (Figure 4a). At this stage the reaction pathway can proceed in one of three routes depending on Ti layer thickness:

(i) Thin (<5 nm) Ti layer (Figure 5a): all Ti converted to TiO_2. By completely consuming metallic Ti, its adhesive benefits are lost and AAO template detaches from underlying noble metal layer. O_2 evolution occurs at Au.

(ii) Intermediate (5-20 nm) Ti layer (Figure 5b): Ti partially converted to TiO_2. Ti directly beneath the pore is anodized but Ti beneath pore walls remains, bridging Al_2O_3/TiO_2 to Au base.

(iii) Thick (>20 nm) Ti layer (Figure 5c): Ti forms TiO_2 barrier layer which cannot propagate further through thick Ti under the experimental conditions (no dissolution).

Clearly, pathway (ii) is optimal and following it the normally unfavorable oxygen evolution reaction (OER) can be advantageous for subsequent pore opening. Pressure from O_2 bubbles formed by this reaction begin to develop the so-called "void" region between oxide (Al_2O_3 or TiO_2) and metal (Au or Pt) whereby the concave pore base becomes inverted. The overanodization method is employed to increase the volume of this void to a critical level where facile barrier etching is possible in the next step; however, allowing the anodization to proceed too long (beyond 10 minutes in our experiments) results in complete AAO detachment. Similar

experiments performed on substrates with the “thin” or “thick” Ti adhesion layers reported above could not be reproducibly anodized to through-hole supported AAO due to template detachment or inability to penetrate the barrier layer, respectively. Here, we highlight the critical thickness of Ti adhesion layers bridging AAO and Au/Pt on Si, adding to the analysis of Liu et al for the Ti adhesion anodization behavior in the AAO/ITO substrate [19]. We also observed a wider range and thicker tolerance level of the Ti adhesion layer for our substrates (5-20 nm compared to 5 nm in earlier work [19]).

A typical etching step follows in order to widen the pores and thin the barrier layer. We explored the possibility of this chemical dissolution as the final step to through-hole morphology since it has been reported to sufficiently etch away the barrier by some authors [1,12]. However, the inherent anisotropy of the chemical etching method did not selectively dissolve the barrier layer before the pore sidewalls, as their thicknesses were quite similar (50 nm and 55 nm, respectively). Therefore, a reversed potential bias was applied relative to anodization for electrochemical barrier dissolution following chemical etching. The substrate’s cathodic bias drives protons from the acidic solution to tunnel through the remaining alumina barrier. Through a mechanism analogous to the OER, they reach the interstitial void and combine to form H_2 (Figure 4b). We propose that the pressure build up from this hydrogen evolution reaction (HER) in the voids beneath the barrier layer along with acidic proton tunneling from above result in localized alumina dissolution to reveal the metal base. The current during reversed bias is initially very low when the insulating barrier layer is intact (Figure. 2, domain 1r) followed by a gradual increase in current where pores begin to open (2r). Finally, all pores quickly open and H_2 bubbles emerge from the substrate’s surface indicating barrier layer removal (Figure 2, domain 3r); proceeding beyond this point results in AAO detachment.

The resultant AAO template, shown for the Ti/Au/Si substrate in Figure 6, has pores with dimensions of 70 nm diameter and 3.2 μm length (aspect ratio = 45). Platinum nanowires deposited into the pores were well-ordered and adhered to the substrate, independent of underlying metal layer (Figure 7 a and b). The wire aggregation effect is due to the high aspect ratio of the wires and their electrostatic interactions to minimize free energy upon template removal in alkaline solutions. Nevertheless, orthogonalization by nanostructuring yields a 70 fold increase in peak current density for methanol oxidation compared to planar platinum (Figure 8).

Conclusions

The method described herein presents an attractive approach for integration of AAO templates with Si to produce 1-dimensional nanostructure arrays. Reproducibly generating these templates requires careful substrate preparation, anodization control, and barrier layer etching. Pt deposited in nanowire arrays exhibits a dramatically increased activity towards methanol oxidation for use in μDMFCs. Further applications are easily envisioned where high surface area nanowire arrays supported on a current collector integrated with Si are desired.

Acknowledgment

The authors acknowledge the Enterprise Ireland funded Technology Development Project CFTD/07/325. We thank Mr. Vince Lodge for recording SEM images. The SEM was funded by "INSPIRE" Higher Education Authority via PRTLI4.

Figure Legend

Figure 1. SEM micrograph of ordered AAO template on Ti/Au/Si with inverted barrier layer after anodization. Inset: top-down view of template displaying hexagonal lattice.

Figure 2. Relative current-time curves during anodization (40 V) and reversed bias (-10 V) steps with regimes labeled: (1a) Oxide formation, pore initiation, (2a) oxide formation/dissolution in equilibrium, (3a) Overanodization with OER, detachment follows (1r) Low electron tunneling current, (2r) Pore bases begin to open, some hydrogen evolution, (3r) Through-hole pores formed, detachment follows. This behavior was observed for AAO on Ti/Au/Si and Ti/Pt/Si.

Figure 3. Schematic of barrier layer removal via through-hole pore etching from final stages of anodization to pore opening.

Figure 4. Relevant ion transport in a single Al_2O_3 pore in oxalic acid under (a) anodic and (b) cathodic bias.

Figure 5. Three possible pathways for barrier layer morphology at end of anodization, depending on Ti adhesion layer thickness; cases for (a) thin, (b) medium, and (c) thick Ti layers. Refer to text for detailed explanation.

Figure 6. Cross-section SEM of AAO template after barrier layer removal on Ti/Au/Si substrate.

Figure 7. Cross-sections of Pt nanowire arrays deposited into in-house AAO templates on (a) Ti/Au/Si and (b) Ti/Pt/Si.

Figure 8. Comparison of planar and nanostructured Pt catalysts deposited into home-grown AAO templates on Ti/Au/Si after template removal. CVs recorded in 1 M CH_3OH + 1 M H_2SO_4, at a scan rate of 20 mV s^{-1}. The current density is based on geometric area and the planar electrode was multiplied by 10 for clarity.

References

[1] D. Crouse, Y.H. Lo, A.E. Miller, M. Crouse, Appl. Phys. Lett. 76 (2000) 49-51.

[2] L.C. Nagle, J.F. Rohan, J. Power Sources 185 (2008) 411-418.

[3] G.Q. Lu, C.Y. Wang, T.J. Yen, X. Zhang, Electrochim. Acta 49 (2004) 821-828.

[4] N. Torres, J. Santander, J.P. Esquivel, N. Sabaté, E. Figueras, P. Ivanov, L. Fonseca, I. Gràcia, C. Cané, Sens. Actuators, B 132 (2008) 540-544.

[5] X. Wang, Y.a. Zhou, Q. Zhang, Y. Zhu, L. Liu, J. Micromech. Microeng. 19 (2009) 094012.

[6] J.P. Esquivel, N. Sabaté, J. Santander, N. Torres-Herrero, I. Gràcia, P. Ivanov, L. Fonseca, C. Cané, J. Power Sources 194 (2009) 391-396.

[7] G.E. Thompson, Thin Solid Films 297 (1997) 192-201.

[8] A. Santos, L. Vojkuvka, J. Pallares, J. Ferre-Borrull, L.F. Marsal, J. Electroanal. Chem. 632 (2009) 139-142.

[9] Z. Chen, H.G. Zhang, J. Electrochem. Soc. 152 (2005) D227-D231.

[10] O. Rabin, P.R. Herz, Y.M. Lin, A.I. Akinwande, S.B. Cronin, M.S. Dresselhaus, Adv. Funct. Mater. 13 (2003) 631-638.

[11] Y. Yang, H.L. Chen, Y.F. Mei, J.B. Chen, X.L. Wu, X.M. Bao, Solid State Commun. 123 (2002) 279-282.

[12] M.S. Sander, L.S. Tan, Adv. Funct. Mater. 13 (2003) 393-397.

[13] M.L. Tian, S.Y. Xu, J.G. Wang, N. Kumar, E. Wertz, Q. Li, P.M. Campbell, M.H.W. Chan, T.E. Mallouk, Nano Lett. 5 (2005) 697-703.

[14] K. Kim, M. Kim, S.M. Cho, Mater. Chem. Phys. 96 (2006) 278-282.

[15] G.-Y. Zhao, C.-L. Xu, D.-J. Guo, H. Li, H.-L. Li, Appl. Surf. Sci. 253 (2007) 3242-3246.

[16] H. Asoh, M. Matsuo, M. Yoshihama, S. Ono, Appl. Phys. Lett. 83 (2003) 4408-4410.

[17] S.Z. Chu, K. Wada, S. Inoue, S. Todoroki, J. Electrochem. Soc. 149 (2002) B321-B327.

[18] X.W. Zhao, S.K. Seo, U.J. Lee, K.H. Leez, J. Electrochem. Soc. 154 (2007) C553-C557.

[19] P.A. Liu, V.P. Singh, S. Rajaputra, Nanotechnology 21 (2010).

[20] A.F. Feil, P. Migowski, J. Dupont, L. Amaral, S.R. Teixeira, J. Phys. Chem. C 115 (2011) 7621-7627.

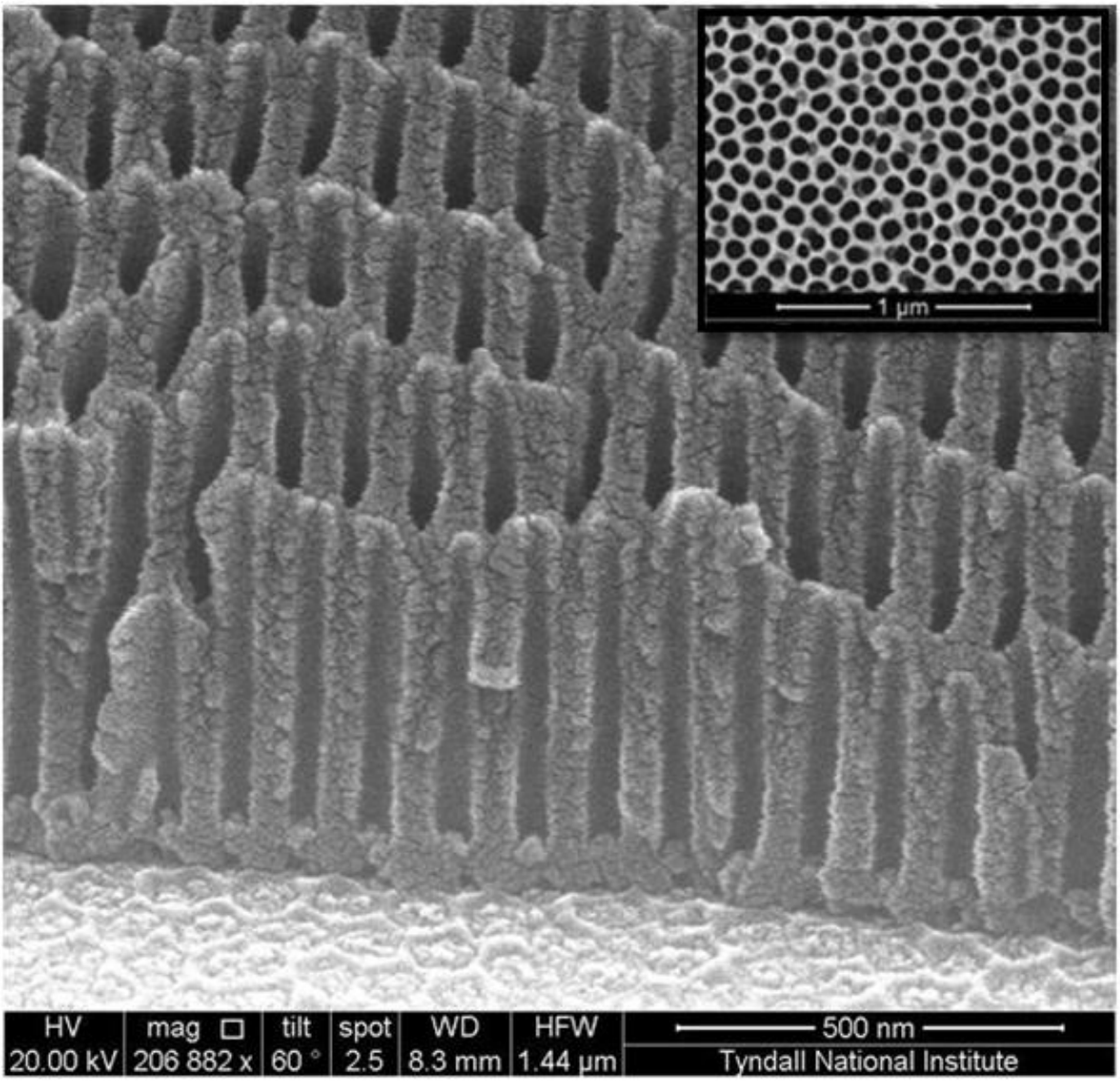

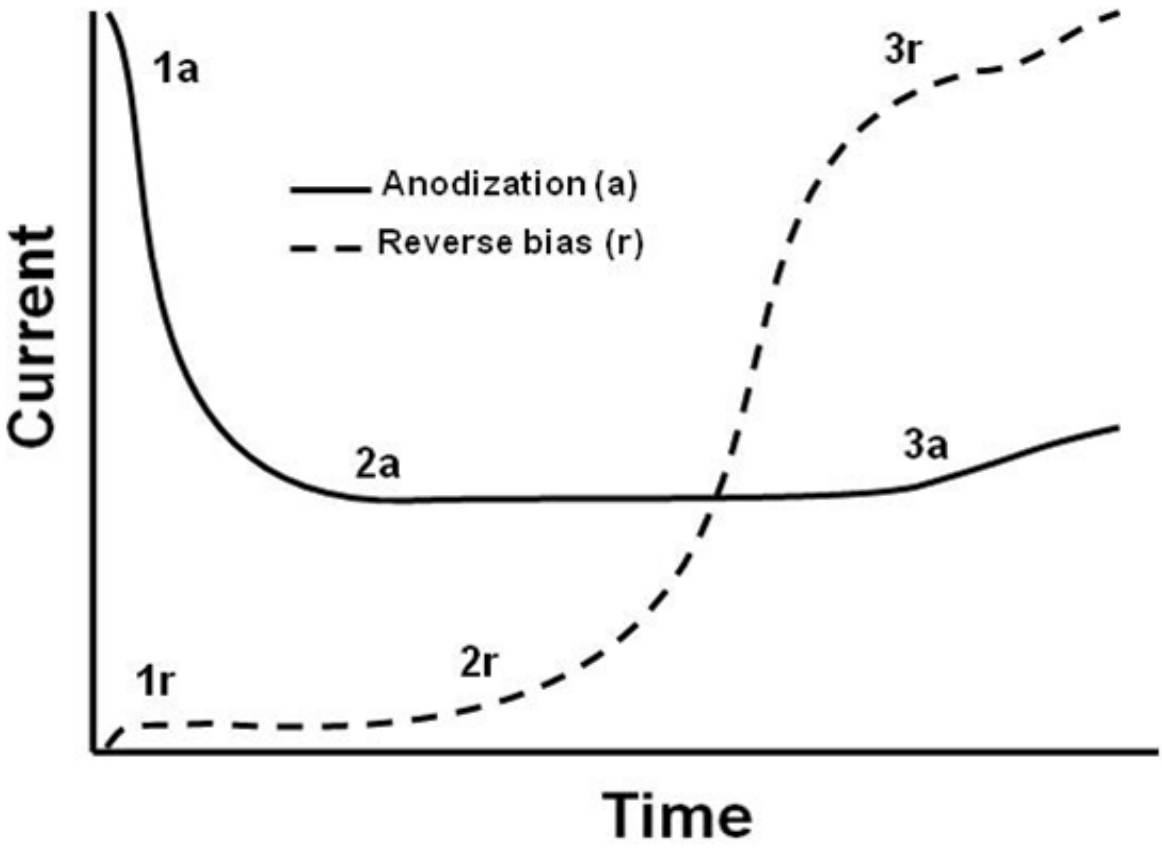

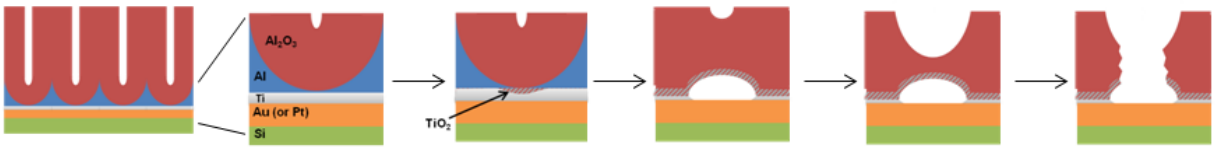

Begin anodization of adhesion layer

Complete, localized anodization of Ti; OER creates void

Widen pores by chemical etch

Remove barrier layer by electrochemical etch

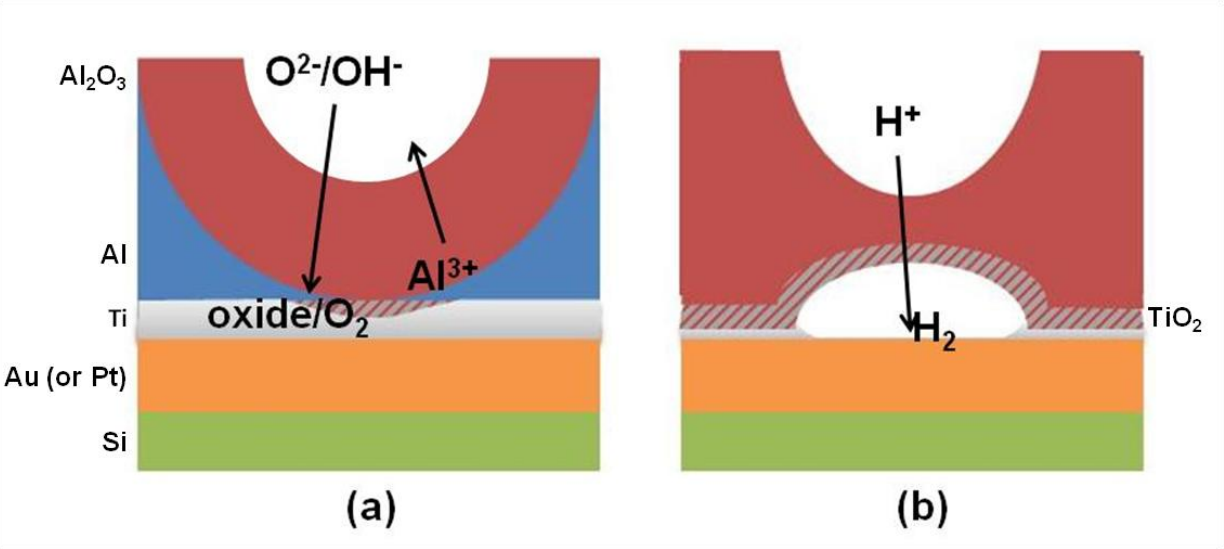
Al_2O_3
O^{2-}/OH^-
Al
Al^{3+}
Ti
oxide/O_2
Au (or Pt)
Si
(a)
H^+
H_2
TiO_2
(b)

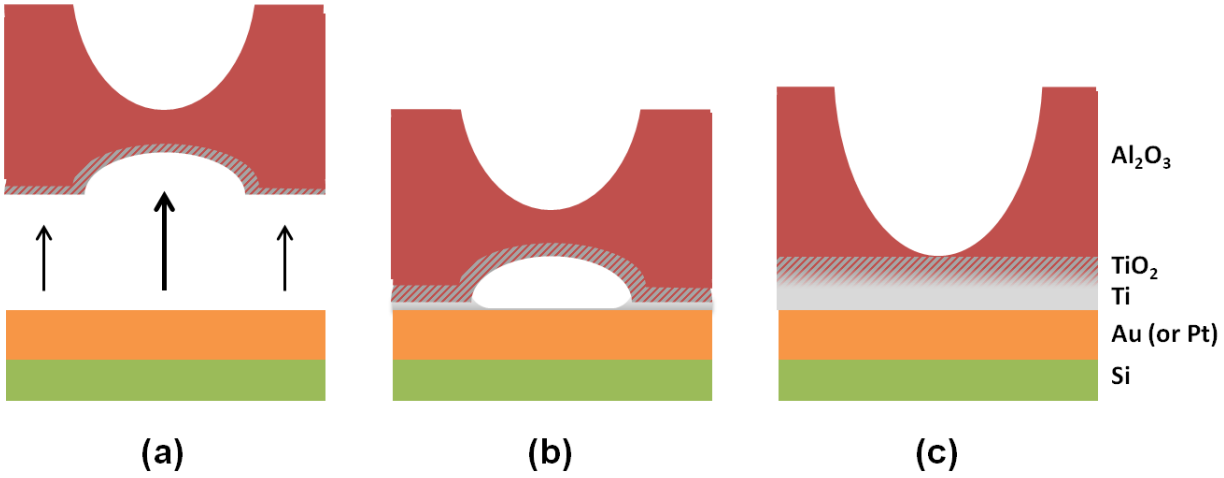
Al_2O_3
TiO_2
Ti
Au (or Pt)
Si
(a)
(b)
(c)

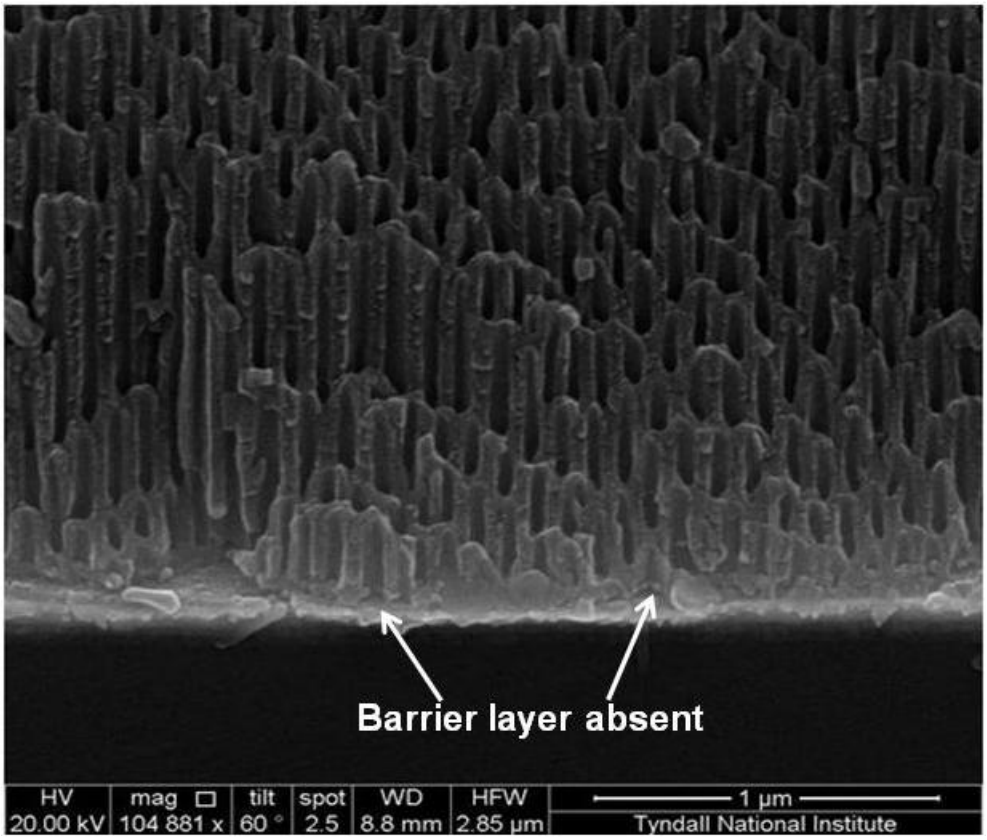
Barrier layer absent
HV
20.00 kV
mag
104 881 x
tilt
60 °
spot
2.5
WD
8.8 mm
HFW
2.85 µm
1 µm
Tyndall National Institute

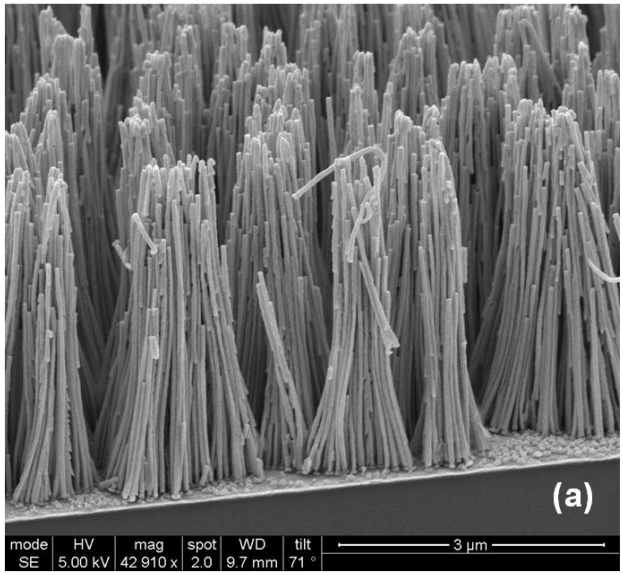
(a)
mode
SE
HV
5.00 kV
mag
42 910 x
spot
2.0
WD
9.7 mm
tilt
71 °
3 µm

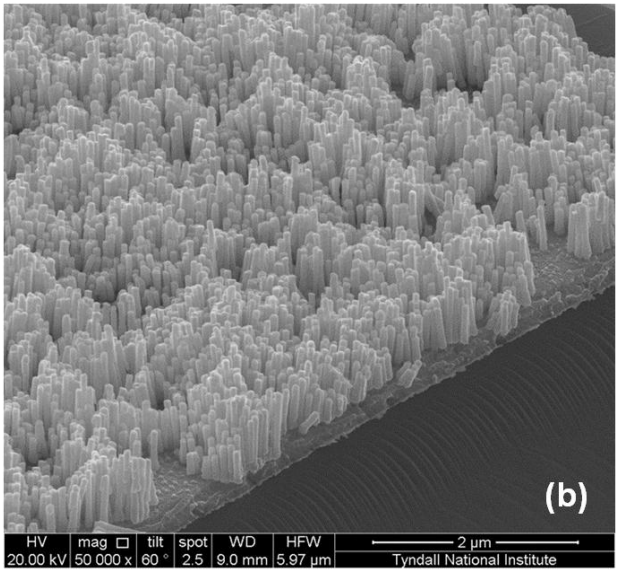
(b)
HV
20.00 kV
mag
50 000 x
tilt
60 °
spot
2.5
WD
9.0 mm
HFW
5.97 µm
2 µm
Tyndall National Institute

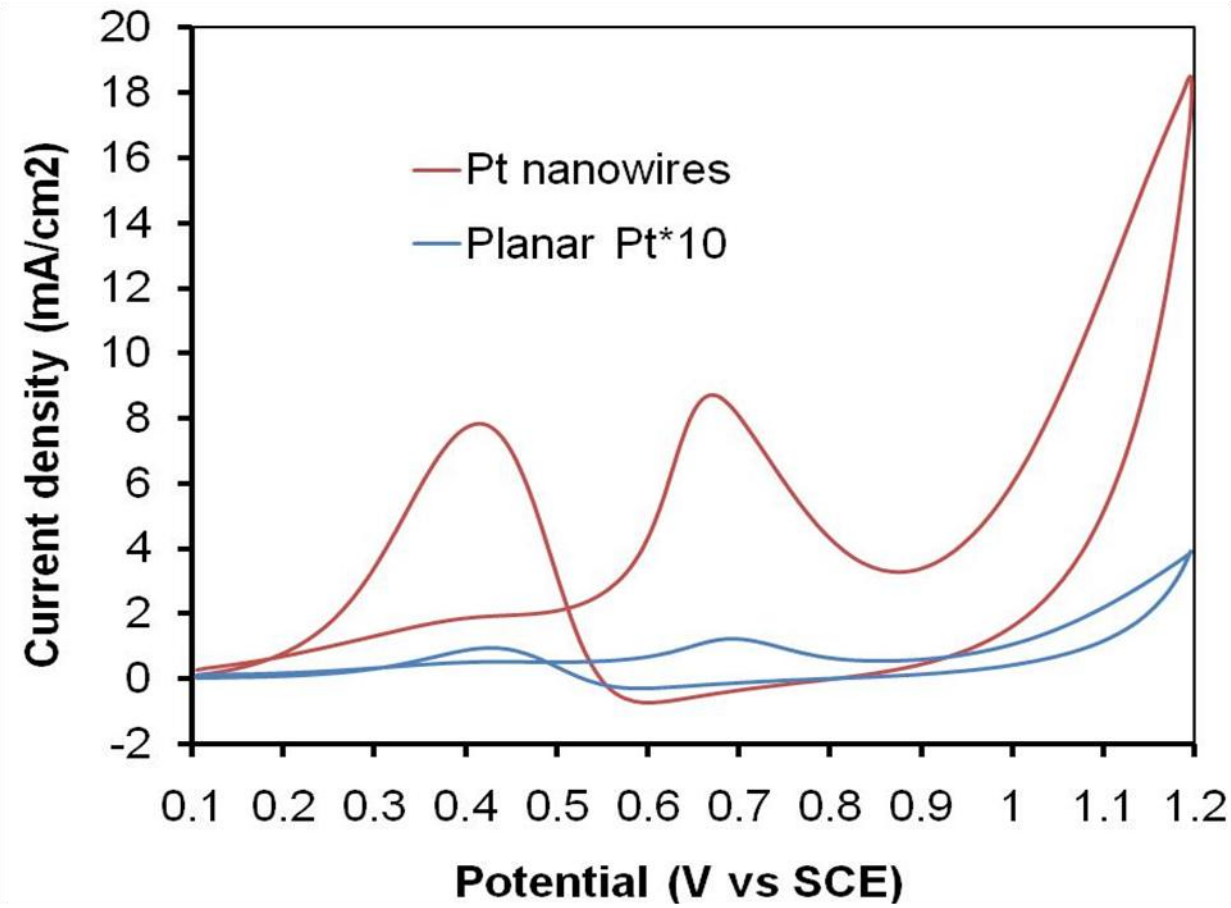
Current density (mA/cm2)
20
18
16
14
12
10
8
6
4
2
0
-2
Pt nanowires
Planar Pt*10
0.1
0.2
0.3
0.4
0.5
0.6
0.7
0.8
0.9
1
1.1
1.2
Potential (V vs SCE)